

¹ PREPARED FOR SUBMISSION TO JINST

² **Directional Xenon Measurement**

³ ABSTRACT: Abstract...

⁴ KEYWORDS: Only keywords from JINST's keywords list please

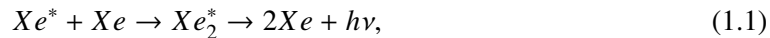
⁵ ARXIV EPRINT: [1234.56789](https://arxiv.org/abs/1234.56789)

| | | | |
|-----------|-----------------|--|-----------|
| 6 | Contents | | |
| 7 | 1 | Introduction | 1 |
| 8 | 2 | Experimental Setup | 2 |
| 9 | 2.1 | Gas handling system | 2 |
| 10 | 2.2 | The Cryogenic system | 3 |
| 11 | 2.3 | The Detector | 5 |
| 12 | 2.3.1 | The Detector Chamber | 5 |
| 13 | 2.3.2 | The Sphere | 6 |
| 14 | 3 | The Data Acquisition (DAQ) System | 8 |
| 15 | 4 | Simulation | 11 |
| 16 | 5 | Summary | 11 |

17 **1** Introduction

18 The use of Noble-liquid detectors in the field of astroparticle physics has increased in the past
19 decades. Detectors aiming at measuring Dark Matter (DM) particles and neutrinos properties use
20 large liquid argon or liquid xenon (LXe) chambers [1, 2]. Current and future experiment for DM
21 detectioin are tuned to detect weakly interacting massive particles (WIMPs), a postulated candiadte
22 for DM particle [3]. LXe based detectors are to date the leading in sensitivity and size for these
23 searches [4–7].

24 When a particle interacts within the LXe media, it forms a cloud of excited and ionized states
25 with typical length of 100 nm. The excited Xe (Xe^*) combines with other Xe atoms to form an
26 excited dimer state (excimer) when they decay to ground state they emit light.



27 The electrons emitted from the ionization can recombine with a surrounding atom, this process of
28 recombination provides another possibility to produce excimers,



29 Once Xe^* is produced it adds to the scintillation process explained in 1.1. There are two types of
30 Xe_2^* excimer states, singlet and triplet, with lifetime of ~ 3 ns and ~ 25 ns respectively. The wave-
31 length emitted by these states is between (175-180) nm which is lower then the lowest excitation of

32 xenon, and therefore travel through it to reach a photo-detector situated outside the LXe. Although
33 much is measured on these scintillation processes, the basic knowledge of the quantum properties
34 of these interactions is based on experiments preformed several decades ago.

35 The phenomenon of superradiance in which identical quantum states "communicate" through
36 electromagnetic field if in close proximity, is well studied. In certain conditions the emission of
37 photons from these correlated states is very different then the sum of random states. This difference
38 is in spectral, temporal and spatial properties [8, 9]. Early studies show that scintillation in LXe can
39 produce coherent amplification of light [10, 11]. These studies were focusing on the macroscopic
40 ionization using high energy density electron beams.

41 The understanding and quantification of the microscopic effects of non linear phenomena such
42 as superradiance in Lxe for a single interaction, can improve DM experiments to reduce back-
43 ground by the extra knowledge of directionality. irreducible background such as coherent neutrino
44 nucleus scattering of neutrinos from the sun can be discard.

45 In this paper we present an experimental set-up called DIREXENO (Directional Xenon) aim-
46 ing at measuring the spatial distribution of LXe scintillation light, and quantify non-isotropic emis-
47 sion.

48 2 Experimental Setup

49 The experimental setup that is described in this section, is designed to measure, the spatial and
50 temporal properties of LXe scintillation. However it is designed in a modular way, so it can serve
51 different requirements from different future experiments.

52 There are four main building blocks constructing the full setup, a schematics of them with
53 the interfaces connecting them is shown in Fig. ???. The gas handling system, which, in normal
54 working mode, drives the xenon from the detector trough a purifier and back into the detector.
55 The cryogenic system, which liquefies the xenon and delivers it to the detector part. The detector
56 system, mainly an HPFS sphere with a small bubble of LXe inside it surrounded with PMTs.
57 Finally the data acquisition (DAQ) system that supplies HV and reads the data from all sensors
58 (e.g., PMTs, pressure gauge etc.). Each building block can be replaced without effecting the others.

59 The full assembly (Fig. 1) is held on three separate wracks, one for the DAQ, while the two
60 others hold the cryogenic detector and gas handling system are joined using a 100mm bar with
61 shock absorbers on both sides. Some of the guidelines for the design of DIREXENO are based
62 on [12]

63 2.1 Gas handling system

64 A typical LXe detector must keep a high level of purity. Careful selection and meticulously clean-
65 ing of all parts before mounting, is needed, however is not sufficient. The desired level of most
66 detectors of impurity concentration is at the level of 1 ppb O_2 equivalent [1]. This is crucial to
67 allow ionization electrons drift for several cm. To reach that level in a reasonable amount of time
68 (several days instead of months), continuous purification is needed. The gas handling system,
69 provides this process, alongside with all gas handling operations such as filling and recuperation.

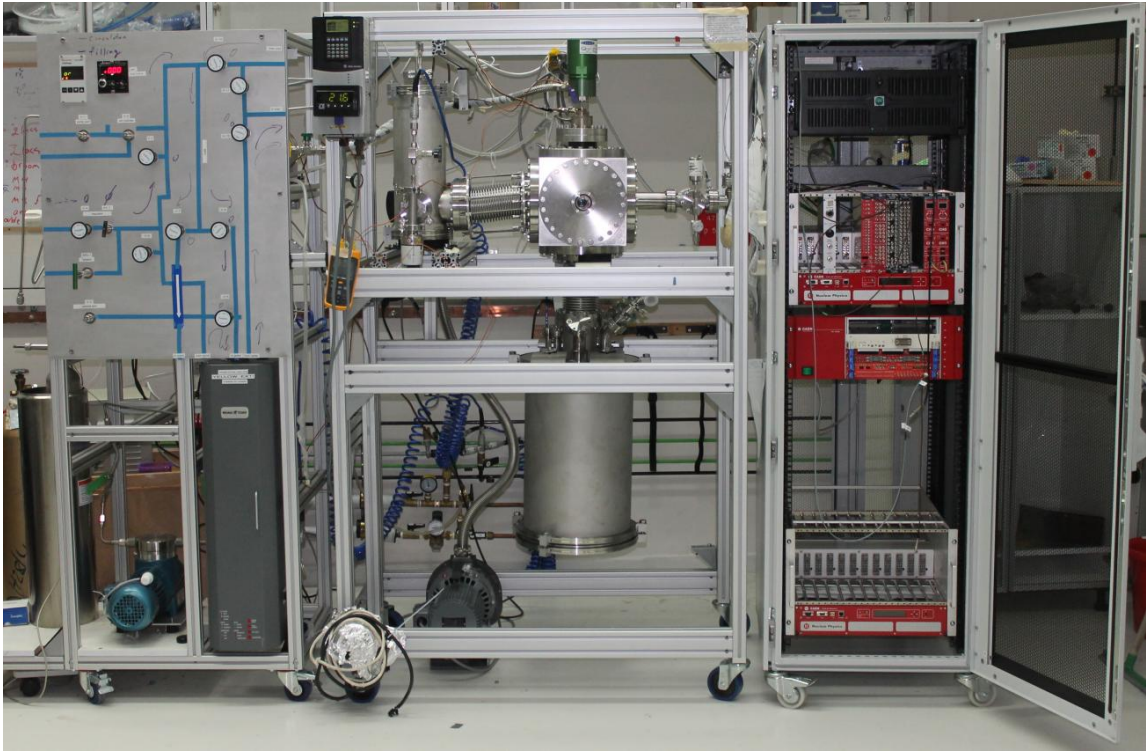


Figure 1. DIREXENO. On the left the purification system, in the middle the cryogenic and detector chamber, and on the right the Data acquisition system.

70 During purification mode, xenon is taken from the chamber (in liquid phase) passes through a
 71 heat exchanger¹ where it is heated and vaporized. The xenon is forced by a KNF diaphragm pump
 72 into a hot getter² which cleans the xenon from most impurities. The xenon also passes through an
 73 MKS Mass Flow Controller³ (MFC), this allows monitoring and controlling the amount of xenon
 74 in the system.

75 After the xenon is purified, it is delivered back to the cryogenic system through the heat ex-
 76 changer, there the remained xenon gas is liquefied before it continues back to the chamber. A
 77 schematic of this system is shown in fig. 2.

78 2.2 The Cryogenic system

79 Remote cooling is generally used in DM experiments due to background radiating from the cooler
 80 to the detector. Although in our system this is not of great importance there are still several ad-
 81 vantages to remote cooling such as: lowering acoustic noise from the cryo-cooler and flexibility to
 82 design changes. The cryogenic system is connected on one side to the gas system and on the other
 83 to the detector chamber, any change in the system (e.g. cooler type or model) requires the change
 84 of that specific part without changing the detector nor the gas system.

¹GEA GBS100M-24 plate heat exchanger

²MONO-TORR PS4-MT15-R-2

³MKS mass flow controller

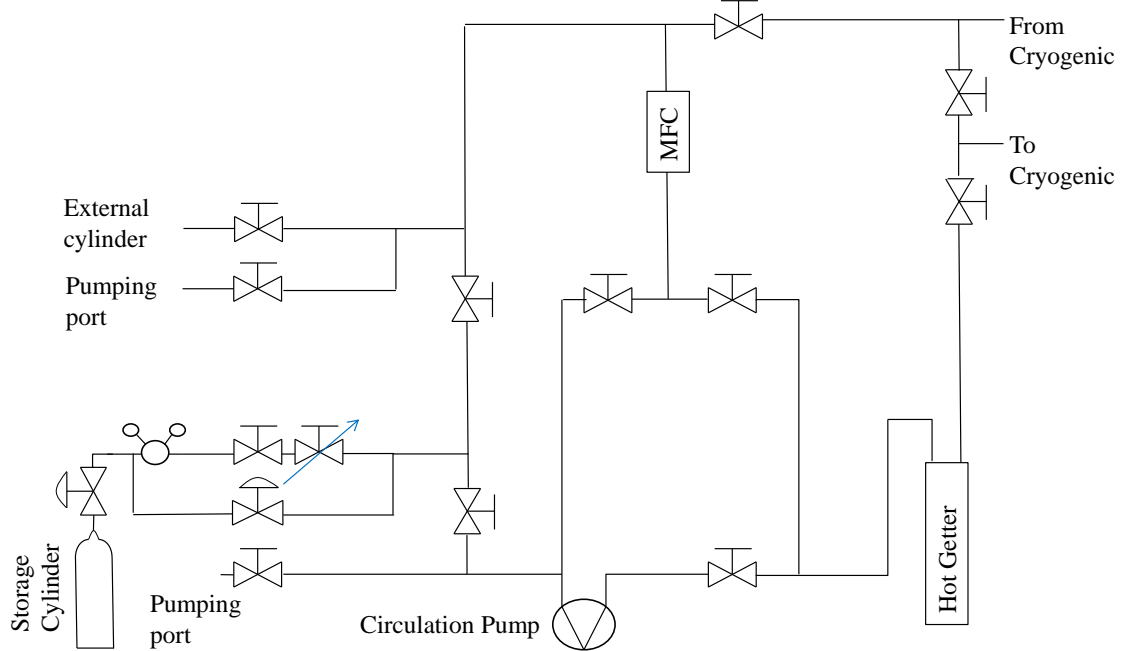


Figure 2. Schematics of the purification system. High pressure valves are indicated as valves with arcs. Needle valves are indicated as a valve with an arrow.

85 The system is made out of two chambers, the outer vessel (OV) which holds the insulation
 86 vacuum, and the inner vessel (IV) that holds the xenon. In addition to the vacuum which prevents
 87 heat leaks from diffusion and convection, the entire IV is covered by multi layer aluminized Mylar
 88 to prevent heating via radiation an image of the detector and the CAD design are shown in Fig 3.

89 The OV is made of a 10" CF cube, with ports on all six faces (e.g., FT, pumping ports, view
 90 ports). This vacuum is shared with the detector one via a 6" CF flexible bellows.

91 The IV is made of 1.5" height cylinder with 6" CF flanges on the top and bottom parts of it,
 92 and it holds inside xenon. A 120 mm diameter cold finger is welded to the top flange of the IV.
 93 The design of the cold finger is similar to the design of [13], the inner part of the cold finger is
 94 made of long fins, therefore the surface area of it is bigger resulting in a better heat transport. The
 95 upper part of the cold finger is in thermal contact with the cryo-cooler ¹ via a cooper adapter. The
 96 copper adapter holds two 100Ω pt resistor which are connected to a PID reader² for temperature
 97 measurements. A Cartridge-heater is also inserted to the copper adapter for emergency heating.

98 The cryo-cooler provides up to 70 W of cooling power, and is connected via a 4½" flange to
 99 the OV top flange, and reaching the IV top flange. Common cryo-coolers used for xenon experi-

¹QDrive 20BB 9p6 A 3 AYNBNCO

²cryo-con model 18i Cryogenic Temp Monitor

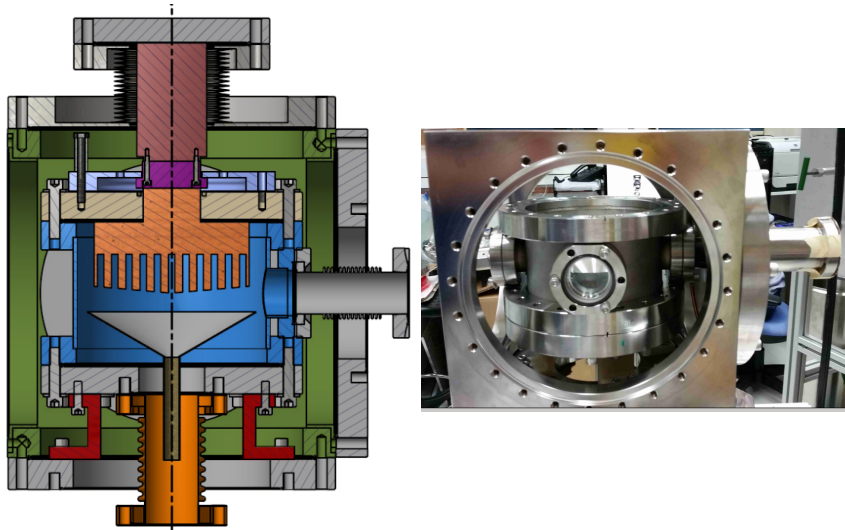


Figure 3. CAD view of the cryogenic system(Left) and a Picture of the cryogenic system (Right) .

ments, work in maximal cooling mode permanently. The QDrive, instead, has temperature control allowing it vary the cooling power, which enables to set the temperature with fluctuations smaller then 0.1 C° on the cooler itself.

On the inner side of the bottom flange of the IV a thin SS funnel is installed collecting all LXe drops from the cold finger, and delivering them to the detector part. This flange is connected to the detector part, via a $3\frac{3}{8}$ " flexible bellows. This bellows hosts two small pipes connected to the circulation system, and a third pipe coming from the funnel, all three pipes deliver LXe whereas the GXe is filling the bellows. The separation between the LXe coming from the gas handling system (clean) and the LXe coming from the cold finger (more dirty) allows the filling of clean LXe to different parts of the detector.

2.3 The Detector

[**MMD:** The detector refers to the chamber and its inner assembly that contains the liquid Xenon bubble, the photomultiplier detectors around it and their accessories. This chamber is placed below the cryogenic system. We describe the detector chamber and its interface to the cryogenic system in section 2.3.1. In section 2.3.2 we discuss the assembly that consists of the HPFS sphere to hold liquid Xenon and the Photomultiplier detectors distributed around the sphere.]

2.3.1 The Detector Chamber

The detector chamber is built such that apart from the interface to the cryogenic system, it can be changed and modified easily for future experiments. The interface unit is built out of 2 flanges welded together via 7 tubes, which serve as service ports for electrical and other feedthroughs. The upper flange, ISO-K NW320, is part of the OV and shares the insulation vacuum of the cryogenic system, the bottom one , CF-8", is part of an IV for future detectors, and would hold xenon inside. For our experiment we modified the CF flange to fit also a $4\frac{5}{8}$ " CF flange which we use.

123 The OV is closed with a cylinder XXX cm height closed from the bottom with another ISO-K
124 NW320 flange, the height of the cylinder is determined such that the maximal height of the whole
125 apparatus is 190 cm, allowing the mobility of the detector through standard doors.

126 The 4 $\frac{5}{8}$ " CF flange is connected to a closed vessel internally divided into two parts. This vessel
127 serves as a xenon reservoir. The two parts of the vessel are connected to a spherical orb from above
128 (inner part) and from below (outer part). LXe is circulated such that new LXe drips into the outer
129 part and pumped from the inner one. This way the liquid level is controlled, and the sphere itself is
130 always filled with LXe.

131 2.3.2 The Sphere

132 The central component of the detector assembly is the hollow sphere which holds the LXe target
133 bubble. A spherical shell made of high purity fused silica with high transmittance is designed to
134 hold the LXe target. The xenon will be circulated Two invar tubes are connected to it from the top
135 and bottom with SS mini-CF flanges at the end, to circulate the xenon (see Fig. \sim 6). The bottom
136 flange of the sphere is held using a brass holder to prevent force or torque applied on the sphere
137 while mounting the detector. The brass holder is connected to a plate held from the top 8" flange,
138 and is also used to align this plate at first installation. A set of 20 PMTs¹r8520-406 Hamamatsu 1"
139 PMT} are placed around the sphere to detect light emitted from the LXe.

140 The LXe target bubble should not be too large in order to avoid double scatters. This shell
141 should be large enough to reduce internal reflections, but not too large which would attenuate the
142 scintillation light. The material of the shell should have a refractive index similar to LXe in order
143 to have minimal diffraction from the original direction of the photons when they travel from the
144 LXe target to the sphere. We chose corning HPFS 8655 as the shell material. The refractive index
145 of HPFS 8655 is 1.575 at 185 nm (LXe R.I. 1.61). In Fig. 4, are the refractive indices at various
146 wavelengths as given by the HPFS factsheet and also a naive extrapolation at lower wavelengths
147 which are relevant to us.

148 The transmittance of the material is extremely crucial for us to optimize the dimension of the
149 shell. Therefore, we obtained a 6 mm thick sample of HPFS 8655 and performed a transmittance
150 testing a VUV monochromator setup. A deuterium light source was used to generate a spectrum
151 in the range (110 - 950) nm, peaked approximately at 160 nm. The window of the light source
152 faced a vacuum space pumped to below 10^{-4} Torr. The monochromator allows to select the desired
153 wavelengths using a manually rotatable holographic diffraction grating. A PMT placed in the
154 vacuum measured the intensity of light emitted from the monochromator, with and without the
155 fused silica sample. The ratio of measured intensities was used to calculate the transmittance of
156 the material. In fig. 5 is the measured transmittances/ 6 mm at (150 - 215) nm. At 175 nm the
157 sample shows approximately 90%/6mm measured transmittance which corresponds to an intrinsic
158 transmittance of about 98%.

159 The dimension of the fused silica shell is optimized by studying the path of the scintillation
160 photons using a GEANT4 based simulation [14]. The sources that will be used for exciting the
161 xenon, and creating the superradiance (signal) as well as the standard emission (background), will
162 be ^{137}Cs (662 keV) and ^{57}Co (122keV & 136 keV) for ER and $^{241}\text{AmBe}$, D-D neutron generator,

¹{

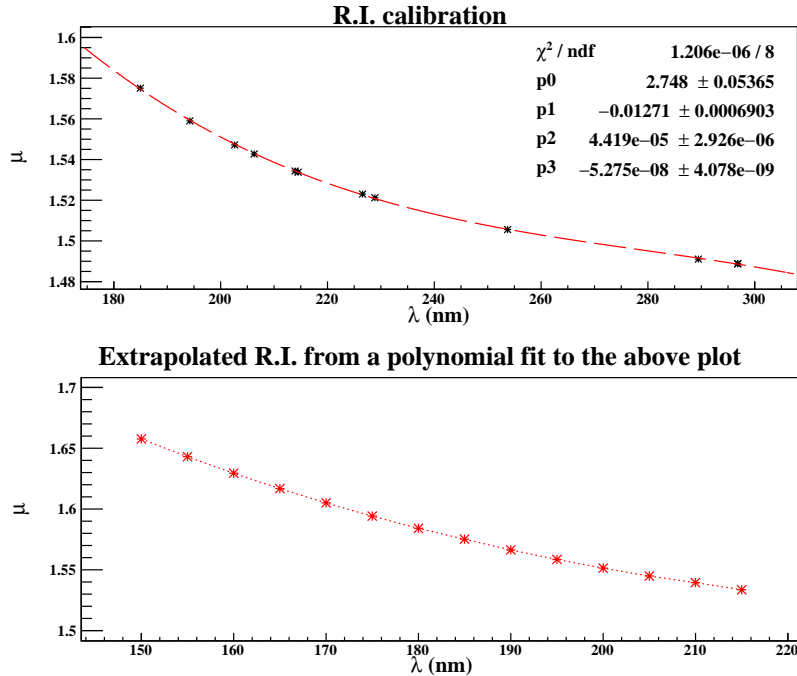


Figure 4. The refractive indices of HPFS 8655 at various wavelengths. (Top) The values provided from Corning factsheet. (Bottom) The values extrapolated at lower wavelengths.

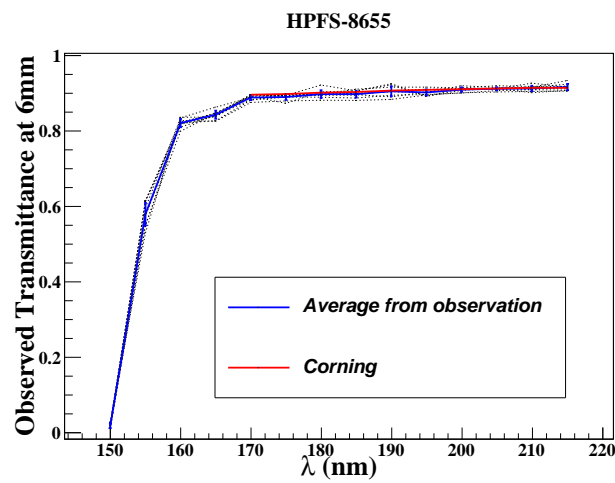


Figure 5. The transmittance of a 6 mm thick HPFS 8655 sample.

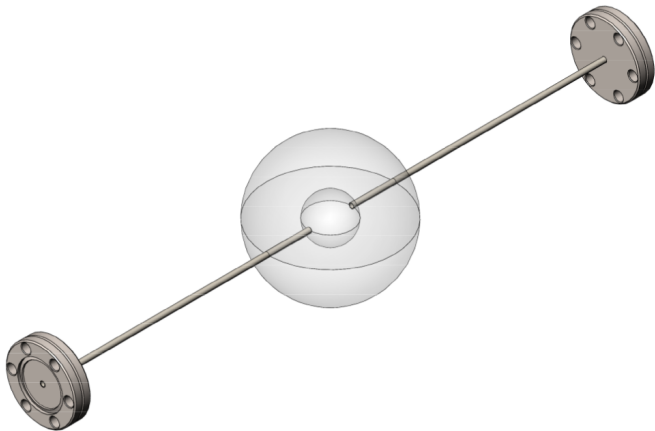


Figure 6. The technical scheme of the HPFS shell with invar tubing and flanges.

or neutron produced in an accelerator for NR . The mean free path for this energy is a couple of mm (^{57}Co) and (0.5 - 3) cm (^{137}Cs). We discuss the simulation in detail in section 4. The outer radius of the shell is 3 cm, while the inner radius of the hollow space that will hold the LXe is 1 cm. The flow of the LXe will be maintained by two invar tubes. This shell–system, as is shown in Fig. 6 is being manufactured industrially as per the specification provided by us.

The photons coming out of the system will be detected by twenty 1" square Hamamatsu R8520-406 photomultiplier tubes with an active area of 20.5 mm \times 20.5 mm each. We pick PMTs with a minimum quantum efficiency of 30% at 178 nm. For an applied voltage of 900 V the gain of these PMTs are 2×10^6 . We use a positive voltage divider, also manufactured by Hamamatsu, to provide high voltage to the PMTs. These 20 PMTs are held with a special aluminum holder, coated with anti-reflection substance. The holder is made of two hemispheres hosting the PMTs in 3 rows all of them pointing to the center of the fused-silica sphere. the PMTs are held only via their voltage–divider bases. The bases are held using M2 PEEK screws. In Fig. 7, one of the holder–hemispheres with the PMTs are shown.

In Fig. 8 we present a CAD schematic as well as a real view of the detector part.

3 The Data Acquisition (DAQ) System

[MMD: This part is almost complete, trigger logic details might get changed slightly]

In this section we discuss the data acquisition and readout from the PMT channels. We use a heterogeneous system consisting of both NIM and VME electronics modules, with the data readout being carried out through the VME controller module V2718 and a PCIe card A3818.

The schematic layout of the DAQ system is shown in Fig. 9. All the 20 PMTs are oriented in the holder assembly which was discussed in section—. The PMTs are ramped up to +800V (the maximum is +900V) using a 24 channel VME high voltage distributor module (VDS18130p) from iseg. The voltage is monitored by the GUI-based control software provided by iseg. For clarity in understanding, we define the raw electrical pulse output of the PMTs as S_i (raw), where $i = 1 - 20$. These raw pulses are then amplified and shaped using two NIM photomultiplier preampli-

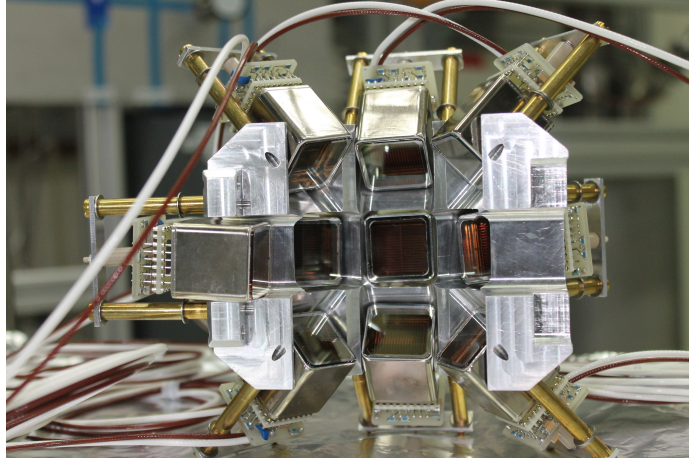


Figure 7. A PMT holder–hemisphere. We use two such components to hold 20 PMTS around the target.



Figure 8. (Left) CAD design of the detector part. (Right) First mounting of the detector part, still not connected to the rest of the system.

189 fiers (Phillips 776). Each of the preamplifier model provides 16 independent and direct-coupled
 190 amplifiers channels. The preamplifier channels operates from DC to 275 MHz and produce two
 191 identical $50\ \Omega$ non inverting outputs with voltage gains of 10. We term **define** the amplified pulses
 192 as S_i , ($i = 1 - 20$). One of the two identical analog outputs from each channel is **What is this word**
 193 **ereingconverted** to a digital signal with an Analog to Digitizer converter (ADC V1742).

194 The ADC module V1742 is a VME board with two 12bit 5GS/s Switched capacitor Digitizer
 195 sections, each of them with 16+1 channels, based on DRS4 chip. The dynamic range of the input
 196 signal is 1 Vpp with adjustable DC offset. This module can sample either bipolar or unipolar analog
 197 input signal within the dynamic range in a circular analog memory buffer, with default sampling
 198 frequency choices 5GS/s, 2.5 GS/s or 2 GS/s. As soon as a trigger signal reaches, all the analog
 199 memory buffers gets frozen and then gets digitized into a digital memory buffer with a 12 bit
 200 resolution.

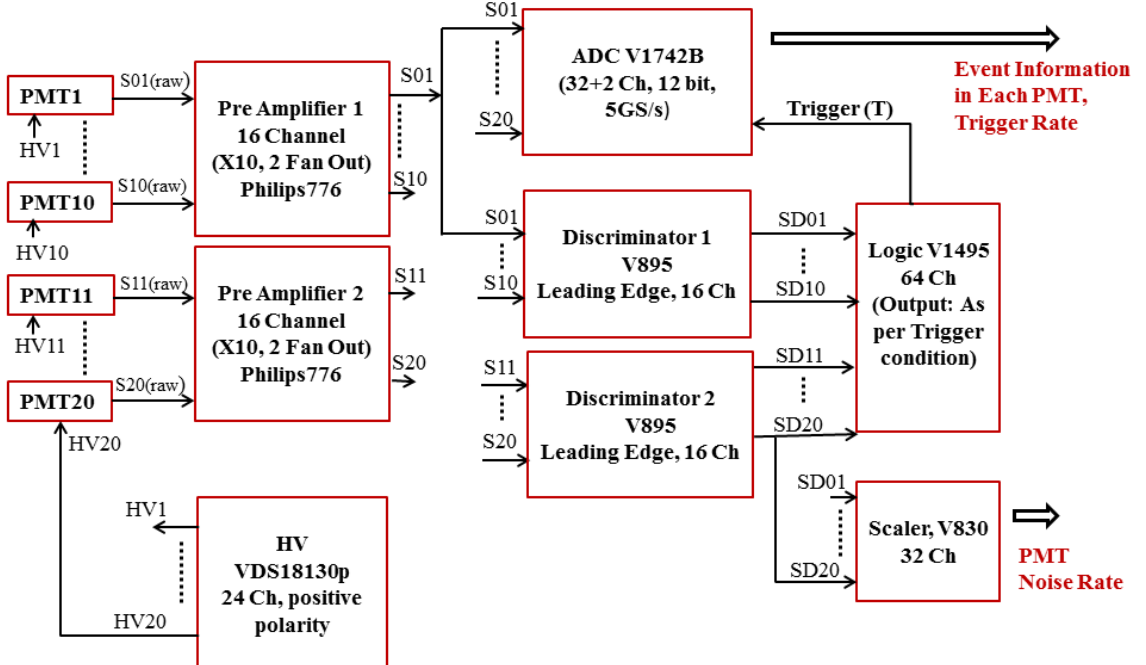


Figure 9. The schematic of the Data Acquisition System of Direxeno. It consists of 20 PMTs and the subsequent electronic channels to record the events for an internal trigger generated by the coincidence of any two PMTs in the system and also the PMT noise rate.

201 We generate an intrinsic trigger for the system, with the coincidence of any two out of the
 202 twenty PMTs. The second output from the preamplifier channels are converted to binary signals
 203 using two 16 channel leading Edge discriminator (V895). In Fig. 9, we term the binary outputs
 204 from V895 as SD_i , $i = 1 - 20$. The SD_i signals are then passed over to v1495, an FPGA based
 205 General purpose VME board which is programmed to perform the logic operation to obtain the
 206 trigger. At present, the coincidence of any two out of the twenty PMTs forms the trigger logic. The
 207 output of V1495 logic operation is used to trigger the ADC V1742 module. In order to record the
 208 PMT noise rate, the SD_i signals are duplicated and fed to a scaler V830.

209 The PMT event information and the trigger rate are read from the ADC, while the Scaler
 210 records the PMT noise rate. The data readout to the acquisition PC is done through the Controller
 211 and optical link to the master PCIe card. The further analyses of the relevant events in the PMTs
 212 will be carried out offline using an analysis framework.

213 **4 Simulation**

214 **5 Summary**

215 **References**

- 216 [1] E. Aprile and T. Doke. Liquid Xenon Detectors for Particle Physics and Astrophysics. *Rev. Mod.*
217 *Phys.*, 82:2053–2097, 2010.
- 218 [2] A. Rubbia. Future liquid Argon detectors. 2013. [*Nucl. Phys. Proc. Suppl.* 235-236, 190(2013)].
- 219 [3] J. Silk et al. *Particle Dark Matter: Observations, Models and Searches*. Cambridge Univ. Press,
220 Cambridge, 2010.
- 221 [4] E. Aprile et al. First Dark Matter Search Results from the XENON1T Experiment. 2017.
- 222 [5] D. S. Akerib et al. Results from a search for dark matter in the complete LUX exposure. *Phys. Rev.*
223 *Lett.*, 118(2):021303, 2017.
- 224 [6] Changbo Fu et al. Spin-Dependent Weakly-Interacting-Massive-ParticleâŠNucleon Cross Section
225 Limits from First Data of PandaX-II Experiment. *Phys. Rev. Lett.*, 118(7):071301, 2017.
- 226 [7] J. Albers et al. DARWIN: towards the ultimate dark matter detector. *JCAP*, 1611:017, 2016.
- 227 [8] R. H. Dicke. Coherence in spontaneous radiation processes. *Phys. Rev.*, 93:99–110, Jan 1954.
- 228 [9] M. Gross and S. Haroche. Superradiance: An essay on the theory of collective spontaneous emission.
229 *Physics Reports*, 93(5):301 – 396, 1982.
- 230 [10] N G Basov, V A Danilychev, and Yurii M Popov. Stimulated emission in the vacuum ultraviolet
231 region. *Soviet Journal of Quantum Electronics*, 1(1):18, 1971.
- 232 [11] Frederick H. Mies. Stimulated emission and population inversion in diatomic bound-continuum
233 transitions. *Molecular Physics*, 26(5):1233–1246, 1973.
- 234 [12] K L Giboni, X Ji, H Lin, A Tan, T Ye, Y Zhang, and L Zhao. A liquid xenon development and test
235 system. *Journal of Instrumentation*, 9(04):T04006, 2014.
- 236 [13] E. Aprile et al. The XENON100 Dark Matter Experiment. *Astropart. Phys.*, 35:573–590, 2012.
- 237 [14] S. Agostinelli et al. GEANT4: A Simulation toolkit. *Nucl. Instrum. Meth.*, A506:250–303, 2003.